

Magnetic properties and quadrupolar interactions in PrAg

P. Morin and D. Schmitt

Laboratoire Louis Néel, Centre National de la Recherche Scientifique,

166X, 38042 Grenoble-Cédex, France

(Received 22 December 1981)

We present an extensive study of the cubic (CsCl-type) rare-earth intermetallic compound PrAg. Numerous experiments have been performed on poly- and monocrystalline samples: neutron spectroscopy, neutron-diffraction, neutron depolarization, resistivity, magnetization, and first- and third-order magnetic susceptibility measurements. Previous determinations of the crystal-field parameters and of the antiferromagnetic structure ($T_N = 10.5$ K) are well confirmed. However, neutron-diffraction and depolarization experiments as well as magnetization curves show the existence of an additional weak ferromagnetic component below $T_c = 6.9$ K. On the other hand, third-order magnetic susceptibility measurements along [001] and [111] axes have been analyzed within an analytical formalism: They reveal the presence of strong negative quadrupolar interactions, which favor a noncollinear arrangement for the magnetic moments.

I. INTRODUCTION

The rare-earth intermetallic compound PrAg has the cubic CsCl-type structure¹ with a lattice constant $a = 3.718$ Å at $T = 4.2$ K. Several experiments on its magnetic properties have been performed in the last two decades, with apparently inconsistent results. In the two first papers^{2,3} it is claimed that the field and temperature dependence of the magnetization indicates a ferromagnetic behavior below 14 K. Some years later, powder neutron-diffraction experiments⁴ showed the existence of an antiferromagnetic ($\pi\pi 0$)-type structure below 14 K. Later other magnetic and neutron-diffraction measurements on a polycrystalline sample confirmed this assumption, giving an ordering temperature of 11 K.^{5,6}

In fact, these ambiguities in PrAg correspond to its location among the RAg series. Indeed, most of the RAg compounds order antiferromagnetically with the ($\pi\pi 0$)-type structure [$R = \text{Nd}$ (Ref. 7), Tb (Ref. 8), Dy (Ref. 9), Ho (Ref. 10), Er (Ref. 11), Tm (Ref. 12)]; the only exception until now is CeAg, which is a ferromagnet with peculiar properties.^{13,14} Thus PrAg lies at the boundary between the domains of stability of the ferro- and antiferromagnetic phases.

Such a balanced competition between ferro- and antiferromagnetic (isotropic) bilinear interactions

may be strongly influenced by (anisotropic) quadrupolar pair interactions, which have been found to be large in rare-earth intermetallic compounds,¹⁵ especially for Pr^{3+} and Tm^{3+} ions. They are then involved in the actual magnetic structures as well as in the moment directions.

All these reasons motivated us to perform numerous types of experiments in order to state all the magnetic properties of PrAg precisely. Resistivity measurements, elastic and inelastic neutron scattering experiments, and a neutron depolarization study have been carried out on polycrystalline material (Sec. II). The first-order magnetic susceptibility as well as the anisotropic behavior of the third-order paramagnetic susceptibility and of the magnetization processes in the ordered and nonordered phases has been studied on a single crystal, the magnetic field being applied along the three main crystallographic directions (Sec. III). In particular, one of our aims was the analysis of the temperature dependence of the third-order magnetic susceptibility in terms of quadrupolar interactions by means of an analytical formalism.¹⁶ This provides the two independent quadrupolar parameters, respectively associated with the tetragonal and trigonal symmetry lowering modes. This type of analysis seems to be more rigorous than a previous interpretation of the magnetic properties of a PrAg polycrystalline sample in terms of purely isotropic biquadratic exchange coupling.⁶

II. EXPERIMENTS ON POLYCRYSTALLINE PrAg

The polycrystalline samples were prepared by the direct fusion of the stoichiometric amounts in a cold crucible. As with samples previously studied in the literature, they were systematically annealed during several hours at 600°C; this precaution was taken to avoid a possible change of magnetic structure before and after annealing, as is the case, for example, in HoAg.¹⁰

Four types of experiments were carried out in order to state the magnetic properties and the crystalline electric field (CEF) precisely: (i) resistivity measurements, giving the temperature and the nature of the transition with accuracy; (ii) neutron spectroscopy, for a confirmation of the previous CEF scheme; (iii) neutron diffraction, for having

more detailed information about the magnetic structure; (iv) neutron depolarization analysis, for investigating the ferromagnetic behavior.

A. Resistivity measurements

Several samples were studied before and after annealing, between 4.2 and 250 K, with particular attention to the range 4.2–15 K. No appreciable amelioration was detected after annealing. In particular, one sample was spark cut with the shape of a staggered grid in order to obtain better accuracy.

The low-temperature part of the resistivity as well as its temperature derivative presents an anomaly at a critical temperature $T_N = 10.5$ K [Fig. 1(a)]. For the temperature derivative, the anomaly at T_N is of λ type, a characteristic of a

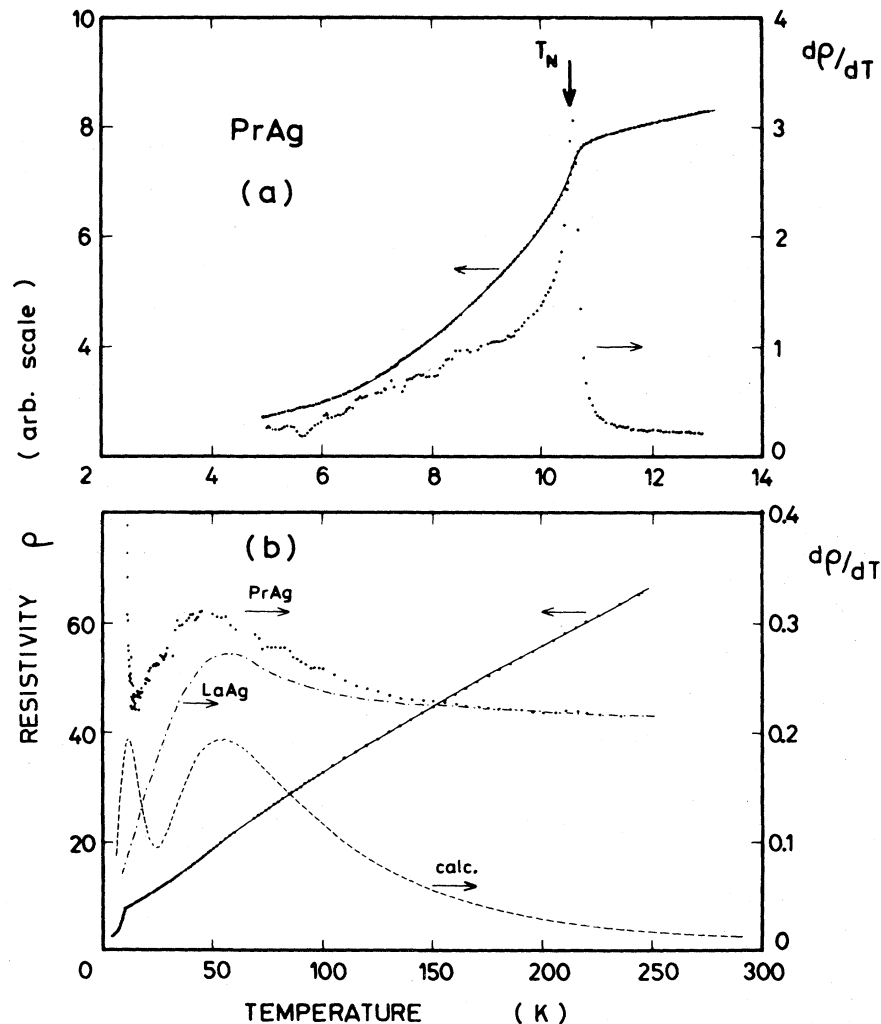


FIG. 1. Temperature dependence of the resistivity (left-hand scale) and of its temperature derivative (right-hand scale) in PrAg; semi-dotted line—temperature derivative for LaAg (from Ref. 18), normalized at 250 K; dashed line—calculated magnetic contribution for PrAg (arbitrary scale).

second-order transition.¹⁷ The small fluctuations below 9 K are due to thermal irregularities during the temperature drift. No transition has been detected between 4.2 K and T_N .

Between T_N and 250 K, no other anomaly is detected, except for a slight negative curvature above 50 K. This is more obvious with the temperature derivative of the resistivity [Fig. 1(b)], which exhibits a maximum around 50 K. This behavior is very similar to the case of the nonmagnetic isomorphous compound LaAg (Ref. 18) and is explained when the Fermi level is within the d band and close to a sharp break in the density of states,¹⁹ as it is the case for LaAg from augmented plane-wave (APW) band calculations.²⁰ This point will be discussed again in the next section, in connection with the CEF contribution to the resistivity.

B. Neutron spectroscopy

The experiments were performed on the time-of-flight spectrometer IN4 at the Institut Laue-Langevin in Grenoble, using neutrons of incident energy of 12.6 and 50.4 meV. The elastic resolution (full width at half maximum) was, respectively, 0.67 and 3.2 meV. Numerous detectors positioned at scattering angles between 2.5° and 80° allowed us to identify the CEF and phonon transitions by following the q dependence of their intensity.

The time-of-flight spectra, normalized relatively to the vanadium standard and corrected for background scattering, were converted into the normalized cross section $S(q, E)$:

$$S(q, E) \propto |f(q)|^2 \sum_{i,j} f_i | \langle i | J_1 | j \rangle |^2 \delta(E - E_{ij}),$$

where $f(q)$ is the form factor for the scattering vector q and the summation occurs for the CEF states i and j ; the f_i 's are the normalized Boltzmann occupation factors. In our analysis only the energy position and the relative intensity of the calculated inelastic transitions were taken into consideration. No particular attention was turned to the experimental linewidths.

Spectra were taken at 20 and 40 K in order to follow the temperature dependence of the CEF transition. Typical counting times were 3 h for each spectrum. In the spectrum with the low incident energy at 20 K (Fig. 2), one CEF inelastic line T_1 is observed at 2.8 meV (32.5 K); its intensi-

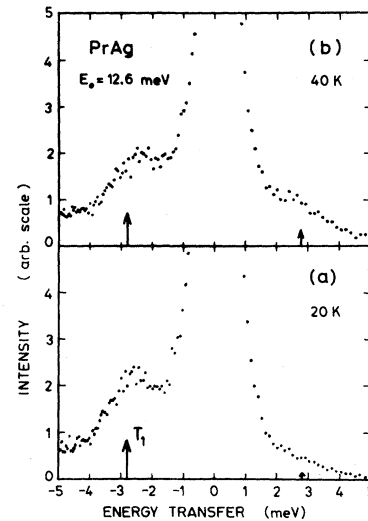


FIG. 2. Normalized time-of-flight spectra for PrAg at (a) 20 K and (b) 40 K with incident energy $E_0 = 12.6$ meV; arrows indicate theoretical position and intensity of the CEF transitions for $W = -5.4$ K, $x = -0.79$.

ty decreases with increasing temperature, while it becomes observable as a deexcitation process when the corresponding excited state is sufficiently populated [Fig. 2(b)].

The spectrum with the high incident energy (Fig. 3) shows two inelastic lines T_2 and T_3 , which are not resolved and which are positioned at 9.5 meV (110 K) and 12.3 meV (143 K), respectively. However, the relative intensity ratio between T_3 and T_2 is inverted when increasing the tempera-

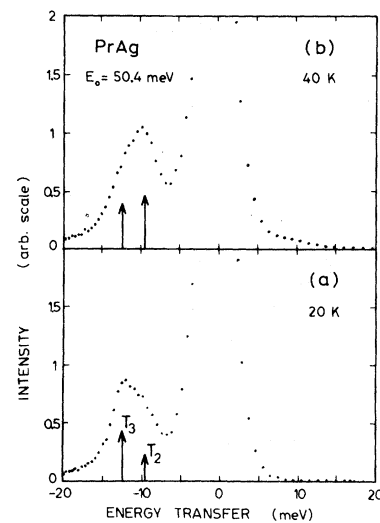


FIG. 3. Normalized time-of-flight spectra for PrAg at (a) 20 K and (b) 40 K with incident energy $E_0 = 50.4$ meV; arrows indicate theoretical position and intensity of the CEF transitions for $W = -5.4$ K, $x = -0.79$.

ture: This means that the 9.5-meV line T_2 corresponds to a transition from an excited CEF level.

In the Lea, Leask, and Wolf diagram²¹ for $J=4$, three solutions are in agreement with the three observed energy transfers for $x = -0.79$, -0.67 , or 0.69 . However, taking into consideration the temperature dependence of the intensities leads to eliminate the two last solutions. The CEF parameters $W = -5.4 \pm 0.2$ K, $x = -0.79 \pm 0.01$ give a perfect agreement with the experiment (see Figs. 2 and 3). The observed inelastic lines then are attributed to the transitions from the ground state Γ_5 to the excited states Γ_3 (T_1) and Γ_4 (T_3), T_2 corresponding to the transition $\Gamma_3 - \Gamma_4$. The usual parameters $A_4 \langle r^4 \rangle = -97$ K, $A_6 \langle r^6 \rangle = -15$ K may be deduced and are consistent in the rare-earth-silver series.^{22,23} This unambiguous solution is also consistent with the literature.^{4,6}

At last we can now come back to the temperature derivative of the resistivity. Starting from the above-mentioned CEF level scheme, the CEF contribution to the resistivity may be calculated²⁴ and its temperature derivative obtained [Fig. 1(b)]: It presents a wide maximum around 50 K and an additional sharp peak around 12 K, which is located in the range of the transition at T_N . However, the difference between the experimental curve and the curve for LaAg (from Ref. 18, normalized at 250 K) does not exhibit any decrease from 50 K down to 25 K, as it would be in the case of a CEF origin. Therefore, the CEF contribution to the resistivity is probably small above T_N , and the observed behavior may arise either from an exciton contribution²⁵ or from an unusual lattice contribution.¹⁸

C. Neutron diffraction

Elastic neutron scattering experiments have been performed on the multidetector of the SILOE neutron reactor at the Centre d'Etudes Nucléaires in Grenoble. Numerous spectra were taken between 2 and 20 K with an incident neutron wavelength of 1.323 Å. The counting times ranged between 1 and 12 h.

First, the main magnetic structure is confirmed with regard to a previous determination⁴: It is antiferromagnetic, with a propagation vector $\vec{q}_{AF} = (\frac{1}{2}, \frac{1}{2}, 0)2\pi/a$. From the temperature dependence of the $(\frac{1}{2}, \frac{1}{2}, 0)$ reflection, the Néel temperature is confirmed to be $T_N = 10.5$ K (Fig. 4). The antiferromagnetic moments reach $M_{AF} = (2.4 \pm 0.2)\mu_B$ at 2 K and lie in the (001) plane with the assumption of a collinear structure [Figs.

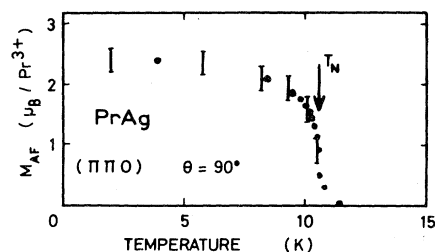


FIG. 4. Temperature variation of the antiferromagnetic moment in PrAg; vertical bars from neutron diffraction on a polycrystal; dots from the $(\frac{1}{2}, \frac{1}{2}, 0)$ reflection of a single crystal (normalized at 4 K).

5(a) and 5(d)]. However, other multiaxis (noncollinear) configurations may exist,^{26,27} giving the same neutron diffraction diagrams; thus, in addition to the collinear configurations with the antiferromagnetic moments within the (001) plane, additional noncollinear configurations are possible with moments along the $[110]$ and $[1\bar{1}0]$ directions [biaxis configuration, Figs. 5(b) and 5(c)], or along the $\langle 111 \rangle$ directions (bi- or quadriaxis configuration, Figs. 5(e) and 5(f)]. However, from the analysis of the nuclear reflections, no distortion has been detected below T_N ; thus PrAg strongly differs from isomorphous antiferromagnets PrZn and PrMg where the tetragonal spontaneous strain exceeds 1%. In these two compounds, analyzing the lattice behavior was enough to deduce that the magnetic structure to be collinear along a fourfold axis.^{28,29} Until now, there exists no thorough systematic study of the magnetoelastic coupling in RAg, but their magnetoelastic coefficients, tetragonal and rhombohedral, may be not too far from the values observed in isomorphous RZn, RCu, and RMg in a way reminiscent of the CEF parameter values. This is confirmed by the spontaneous tetragonal strain (4.5%) observed in TbAg compared to the value 11% in TbCu.³⁰ Within this as-

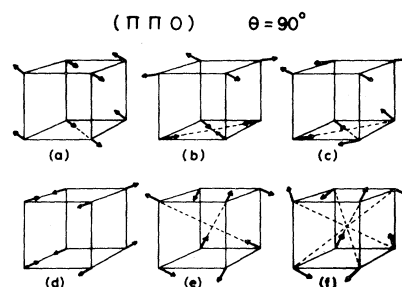


FIG. 5. Possible configurations for the $(\pi\pi 0)$ -type antiferromagnetic structure with $\theta=90^\circ$: (a) and (d) collinear; (b), (c), and (e) biaxis; (f) multiaxis.

sumption the corresponding collinear structure [Fig. 5(d)] may appear to be very unlikely in PrAg. The strain induced by moments pointing along twofold or threefold axes is usually very small in CsCl-type compounds as observed, for example, in TbZn, HoZn,³¹ and NdZn. The lack of a noticeable distortion is not conclusive with regard to the remaining magnetic structures of Fig. 5.

We made also a detailed analysis of the weak superstructure nuclear reflections [(100), (111), and (210)]. At 2 K, a very small increase of their intensity occurs relative to the spectra taken at 9 K and above, which corresponds to a ferromagnetic moment $M_F = (0.3 \pm 0.2)\mu_B$. Note the large relative error due to the weakness of the intensity of these lines (with $h+k+1$ odd). Therefore, neutron diffraction results show that a small ferromagnetic component coexists with a large antiferromagnetic component: The magnetic structure is weakly canted. As the ferromagnetic component must be perpendicular to the antiferromagnetic component, it may point along the [001] axis in the case of structures 5(a)–5(c) or along the $[\bar{1}01]$ axis in the case of structure 5(e); the multiaxis structure 5(f) with the moments pointing along the four threefold axes is then to be rejected.

D. Neutron depolarization

In order to confirm the existence of a spontaneous magnetization at low temperature, a neutron depolarization study has been carried out on the D5 spectrometer of the ILL high-flux reactor in Grenoble. When a polarized neutron beam goes through a sample having a ferromagnetic component, a partial depolarization occurs in direct proportion to the magnitude of the moment and the magnetic domain structure.³² Therefore a polycrystalline sample of PrAg has been placed into a polarized neutron beam (flipping ratio $R = 19.7$, neutron wavelength $\lambda = 0.84 \text{ \AA}$), and in a 6-Oe magnetic field (remanent field of the electromagnet). Measurements of the number of depolarized neutrons have been made as a function of the temperature (typical counting time: 10 s).

The result is shown in Fig. 6: A very strong increase of the neutron depolarization occurs below $T_c = 6.9 \pm 0.5 \text{ K}$, a temperature lower than T_N , where, as expected, no anomaly has been detected. The indetermination of the absolute temperature led us to this large error bar on T_c . The flipping ratio reaches $R = 4.7$ at 3 K, indicating that the

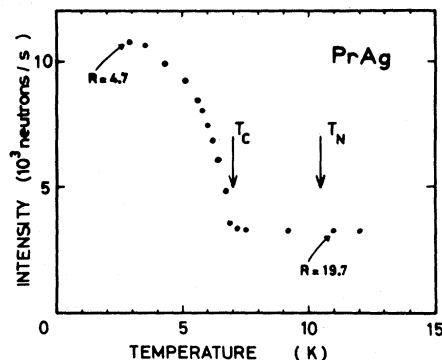


FIG. 6. Temperature variation of the number of depolarized neutrons in PrAg (R is the flipping ratio).

depolarization rate has been multiplied by 3.6 between 8 and 3 K. As the magnetic domain structure is unknown, it is not possible to deduce the ferromagnetic moment value. This experiment proves without ambiguity the existence of a canted temperature T_c in PrAg, below which the existing antiferromagnetic structure begins to close, inducing a weak ferromagnetic component.

III. EXPERIMENTS ON A SINGLE CRYSTAL

The experiments performed on the single crystal have consisted of first- and third-order paramagnetic susceptibilities and magnetization measurements along the main crystallographic directions of the cubic symmetry. The sample was a monocrystalline sphere of about 6 mm in diameter, spark cut from an ingot grown in a Bridgman furnace.

A. First-order magnetic susceptibility

In the paramagnetic range the first-order magnetic susceptibility follows a Curie-Weiss law; the reciprocal susceptibility is linear, with a slight change of slope over the investigated temperature range. The effective paramagnetic moment is $3.49\mu_B$ at 50 K and $3.67\mu_B$ at 300 K (the theoretical value for Pr^{3+} is $3.58\mu_B$, if taking into account the 3H_4 multiplet only). The constant vertical separation of the reciprocal susceptibility with regard to the curve calculated with only the above-mentioned CEF parameters arises from a bilinear exchange coupling (Fig. 7). Good agreement is obtained in the range 11–25 K with an isotropic bilinear exchange parameter $\Theta^* = 11.5 \pm 0.5 \text{ K}$. Note this strongly positive value while the structure is essentially antiferromagnetic. This means that the

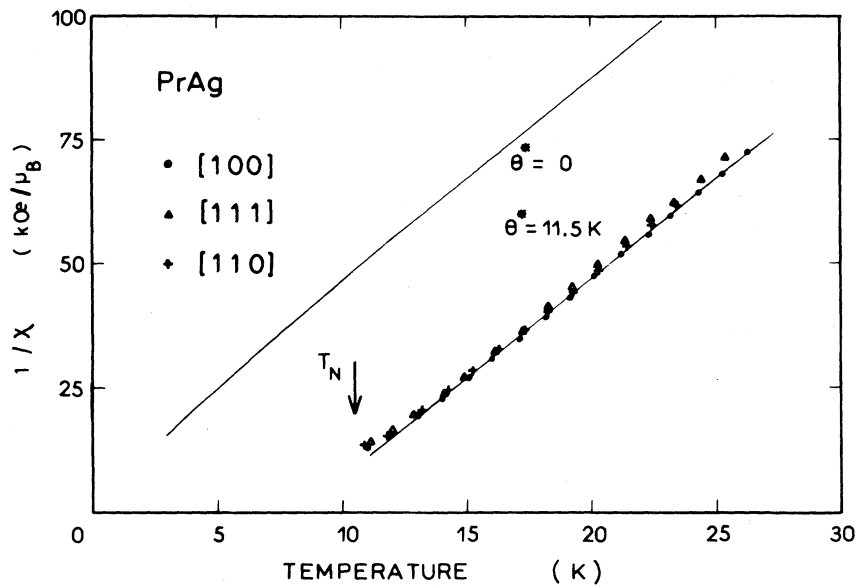


FIG. 7. Temperature variation of the reciprocal first-order magnetic susceptibility in PrAg, along the [100], [110], and [111] directions; lines are theoretical fits for different values of θ^* .

coupling between the $4f$ ions is mainly ferromagnetic, a weak additional antiferromagnetic coupling being sufficient to induce the actual magnetic structure. This also explains the shift of the reciprocal susceptibility towards lower temperatures when diluting Pr by La (Ref. 6): The paramagnetic Curie temperature decreases from 6 K in PrAg to 0 K in $\text{Pr}_{0.5}\text{La}_{0.5}\text{Ag}$.

Below T_N the magnetic susceptibility is anisotro-

pic [Fig. 8(a)], but remains very similar along the [110] and [111] directions with a clear maximum at T_N . Along the [100] direction there is no susceptibility maximum at T_N in a magnetic field of 1045 Oe. However, this maximum occurs in low fields [Fig. 8(b)]. In addition, as a function of the applied magnetic field, M/H exhibits along [100] a behavior characteristic of an antiferromagnetic state above 7 K (increase with H) and of a fer-

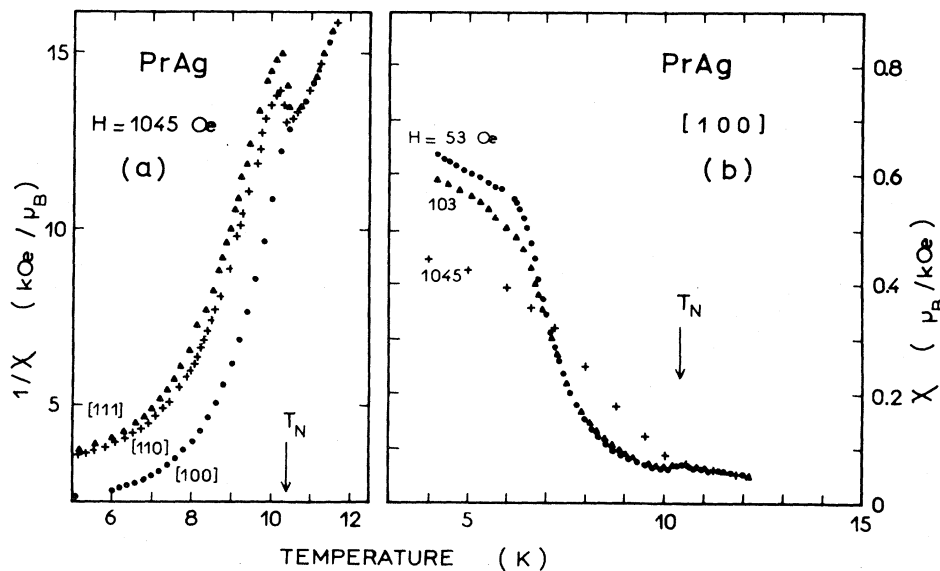


FIG. 8. Reciprocal magnetic susceptibility along three symmetry directions in PrAg; (b) susceptibility along [100] for different fields.

romagnetic one below 7 K (decrease with H). Note that Fig. 1(a) of Ref. 6 shows the existence of a very weak remanent magnetization ($\sim 0.02\mu_B/\text{Pr}^{3+}$) below 7 K, for H reduced from 56 to 0 kOe, on a polycrystalline sample. This agrees with a ferromagnetic behavior.

B. Third-order paramagnetic susceptibility

The third-order magnetic susceptibility has been recently introduced for studying quadrupolar interactions in cubic rare-earth compounds.¹⁶ This method is based on a detailed analysis of the magnetization curves *in the paramagnetic range*. The third-order magnetic susceptibility characterizes the anisotropic initial curvature of the magnetization curves (H^3 term in its field development). A formalism derived from perturbation theory led to its analytical expression in terms of CEF susceptibilities¹⁶:

$$\chi_M^{(3)} = \frac{1}{(1-n\chi_0)^4} \left[\chi_0^{(3)} + 2G_1 \frac{(\chi_2^{(2)})^2}{1-G_1\chi_2} \right] \quad (1)$$

with a magnetic field applied along the [100] direction; χ_0 is the usual (first-order) CEF magnetic susceptibility, χ_2 is the strain susceptibility, $\chi_2^{(2)}$ is the quadrupolar field susceptibility, and $\chi_0^{(3)}$ is the pure CEF third-order magnetic susceptibility. These four CEF susceptibilities may be calculated from the cubic CEF level scheme (see Appendix of Ref. 16). We note that in addition to the enhancement by the isotropic bilinear exchange parameter

$$n = \frac{3\Theta^*}{g^2\mu_B^2J(J+1)},$$

$\chi_M^{(3)}$ receives a contribution from the quadrupolar interactions through the tetragonal quadrupolar parameter G_1 (sum of magnetoelastic and two-ion quadrupolar contributions). The same expression for $\chi_M^{(3)}$ is valid when the field is along the [111] direction, but G_1 has to be replaced by $\frac{1}{12}G_2$, G_2 being the trigonal quadrupolar parameter. Therefore, with the CEF level scheme and the parameter n being known from other experiments (Secs. II B and III A), performing a measurement of $\chi_M^{(3)}$ successively along a [100] and a [111] direction allows us to obtain separately both coefficients G_1 and G_2 .

The values of the third-order magnetic susceptibility were deduced from a detailed analysis of M/H vs H^2 curves, in the temperature range 11–25 K, and for the [100] and [111] directions. These curves are linear in low fields; their extrapolation in zero field gives the first-order magnetic susceptibility while their slope provides $\chi_M^{(3)}$. Their temperature variation is reported in Fig. 9. For the [100] direction [Fig. 9(a)], the fit is not as selective as for previous studies of thulium compounds¹⁶; the value of G_1 is obviously negative ranging between 0 and -1 K. For the [111] direction [Fig. 9(b)], fits are more selective and we can evaluate the trigonal quadrupolar parameter $G_2 = -0.6 \pm 0.2$ K. Note the anisotropy of $\chi_0^{(3)}$ (dotted lines of Fig. 9): As for the other susceptibilities χ_2 and $\chi_2^{(2)}$, this originates from the composition of the Γ_5 ground state, χ_0 remaining isotro-

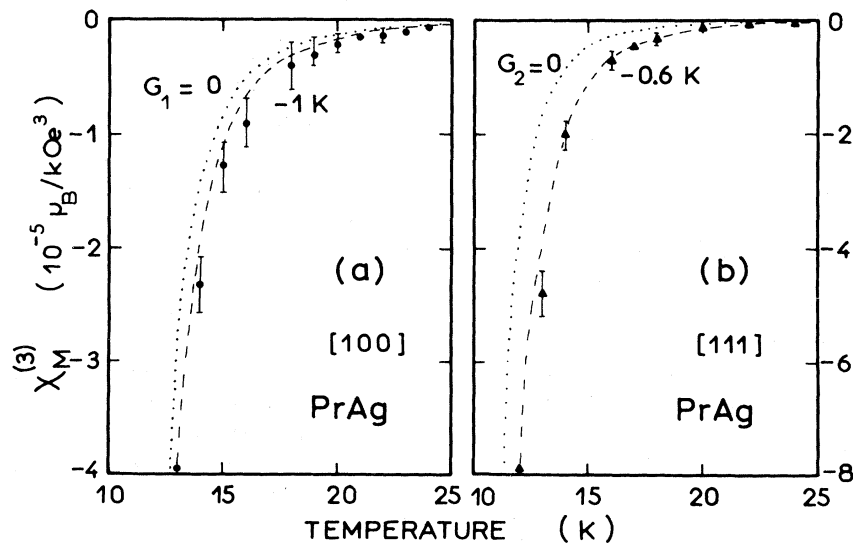


FIG. 9. Third-order magnetic susceptibility along (a) [100] and (b) [111] in PrAg; lines are theoretical fits.

pic in cubic symmetry (see Appendix B in Ref. 16). Thus the weak anisotropy of $\chi_M^{(3)}$ observed in PrAg is due to the anisotropic quadrupolar contribution, which partially cancels the anisotropic behavior of $\chi_0^{(3)}$.

Let us now come back to an alternative analysis of the magnetization curves in the paramagnetic range, which is described in Ref. 6. In this paper, the authors studied the isothermal magnetization of a *polycrystalline* sample of PrAg; they compared the experimental curve M versus the internal field H after demagnetization correction [see, below, the corresponding Eq. (3)] with curve M vs H_{eff} , an effective field acting on each Pr^{3+} ion; these latter curves were calculated from the simple CEF and Zeeman terms, but only along the peculiar [100] axis [see Eq. (7) in Ref. 6]. For a given M , the difference $H_{\text{eff}} - H$ was taken as the net "exchange field" H_{ex} , and it was found that, at each temperature, the dependence of H_{ex} on M contained an isotropic linear term *and also* an isotropic cubic M^3 term:

$$H_{\text{ex}} = \lambda M + \lambda' M^3 + \dots \quad (2)$$

They tried to interpret this λ' coefficient in term of biquadratic exchange coupling; this coupling is isotropic and includes a bilinear contribution.^{33,34} In comparison with (anisotropic) quadrupolar interactions, it only corresponds to the peculiar isotropy case, $G_2 = 12G_1$.¹⁶ Note that the formalism of Ref. 16 takes into account the one-ion magnetoelastic coupling in addition to the quadrupolar pair interactions.

If we want to compare both analyses,^{6,16} we must write the various relations between M , H , H_{eff} , and H_{ex} :

$$M = \chi_M H + \chi_M^{(3)} H^3 + \dots, \quad (3)$$

$$M = \chi_0 H_{\text{eff}} + \chi_0^{(3)} H_{\text{eff}}^3 + \dots, \quad (4)$$

$$H_{\text{ex}} = H_{\text{eff}} - H. \quad (5)$$

Equation (3) expresses the experimental dependence of the magnetization M on the internal field H ; Eq. (4) represents the theoretical development of M versus the effective field H_{eff} , χ_0 , and $\chi_0^{(3)}$ depending only on the CEF scheme. From Eqs. (2)–(5) we can deduce the expressions for χ_M and $\chi_M^{(3)}$:

$$\chi_M = \frac{\chi_0}{1 - \lambda \chi_0}, \quad (6)$$

$$\chi_M^{(3)} = \frac{1}{(1 - \lambda \chi_0)^4} (\chi_0^{(3)} + \lambda' \chi_0^4). \quad (7)$$

Equation (6) shows the identity between λ and

$$n = \frac{3\Theta^*}{g^2 \mu_B^2 J(J+1)},$$

which are temperature independent. The comparison between Eqs. (1) and (7) immediately provides

$$\lambda' = 2G_1 \frac{(\chi_2^{(2)})^2}{\chi_0^4 (1 - G_1 \chi_2)} \quad (8)$$

in the case of an external field applied along a [100] direction, and the same expression with $G_1 \rightarrow \frac{1}{12} G_2$ along a [111] direction. The different temperature dependences of the anisotropic susceptibilities χ_2 , $\chi_2^{(2)}$, and also $\chi_0^{(3)}$ then lead obviously to the anisotropic and temperature-dependent behavior of λ' .

We can now try to analyze the values of λ and λ' in both approaches: (i) As stated above, and verified in Sec. III A, λ must be temperature independent, which is not verified in Fig. 9 of Ref. 6. Instead of $\lambda = 38.4 \text{ kOe}/\mu_B$ as found in our whole temperature range, λ must vary from 36.6 kOe/μ_B at 10 K to 39.1 kOe/μ_B at 14 K to explain the data on the polycrystalline sample of PrAg.⁶ In $\text{Pr}_{0.5}\text{La}_{0.5}\text{Ag}$ the relative variation of λ reaches even 50% between 4 and 10 K. (ii) From our results along the [111] axis and using Eq. (8) (with $G_2 = -0.6 \text{ K}$), the relative T variation of λ'_{111} should be about 25% between 10 K ($\lambda'_{111} = -3.5 \text{ kOe}/\mu_B^3$) and 14 K ($-4.4 \text{ kOe}/\mu_B^3$); for the [100] axis, the relative variation should be of the order of 12% around $-0.5 \text{ kOe}/\mu_B^2$ (with $G_1 = -0.1 \text{ K}$). The corresponding variation given in Ref. 6 is less than 2% around $-6.4 \text{ kOe}/\mu_B^3$, a value which appears to be far from our results. (iii) Note that in a further study of a monocrystalline sample of DySb in the paramagnetic range, the same authors found that the λ bilinear exchange coefficient was temperature independent,³⁵ while the λ' biquadratic one was highly anisotropic and temperature dependent.³⁶

C. Magnetization curves in the ordered range

Magnetization measurements have been performed for the [100], [110], and [111] directions at several temperatures in the ordered state and in fields up to 15 T at the Service National des Champs Intenses in Grenoble. Figure 10 represents the three curves at 1.6 K, showing critical fields, the value of which ranges from 4.5 to 12 T according to the field direction. The amplitude of

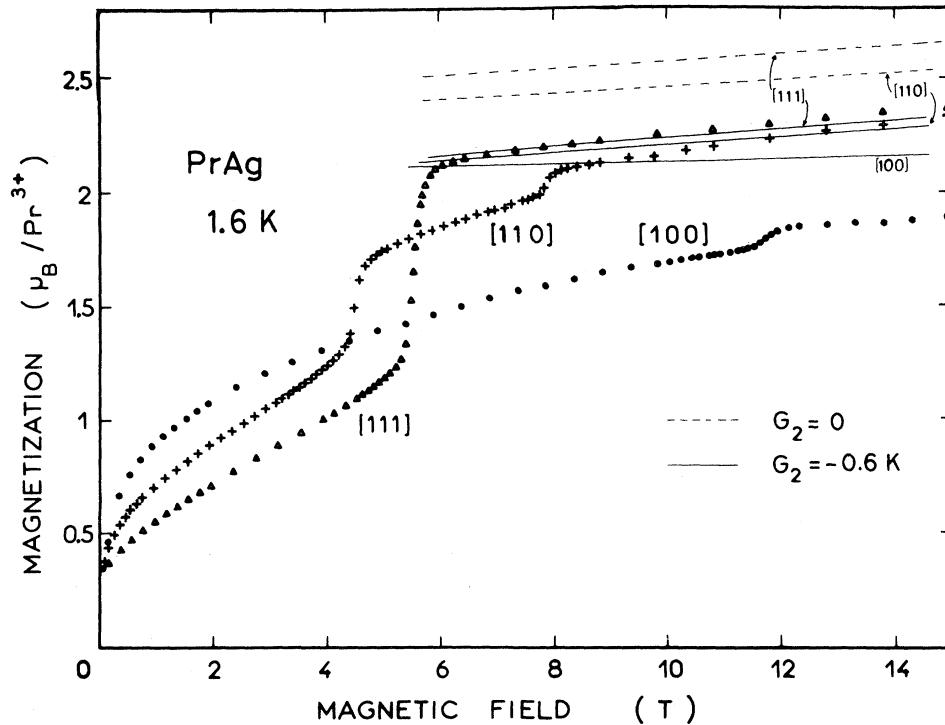


FIG. 10. Magnetization curves along three symmetry directions at 1.6 K in PrAg; dashed lines—theoretical curves with $G_1 = G_2 = 0$; solid lines—theoretical curves with $G_1 = 0$ and $G_2 = -0.6$ K.

the jumps is the largest for the [111] direction and the smallest for the [100] direction, while there are two jumps along the [110] axis. These high critical fields may be associated with spin-flip transitions between the zero-field magnetic structure and either a ferromagnetic state or other intermediate (canted) structures (especially with the field applied along a [110] axis). Note that in Ref. 6, only one critical field was observed at 0.45 T on a polycrystalline sample. In low field, the behavior is reminiscent of the situation in a ferromagnetic with a spontaneous moment of the order of $0.3\mu_B$ (see below).

When increasing the temperature, the critical fields decrease while the amplitude of the jumps decreases (Fig. 11), due to the lowering of the exchange energy. Their temperature dependence is given in the inset of Fig. 11. Two among the four large critical fields vanish at T_N while the two others go to finite values. Note that an additional critical field is observed along [100] in very low field (see below).

The low magnetic field curves (below 0.5 T) present unique features (Fig. 12). At 5 K, a ferromagnetic behavior is observed for the three directions with a spontaneous moment around

$0.2\mu_B$, and the [100] curve shows a critical field of 0.1 T. At 9 K, there is no evidence of a spontaneous magnetization; the curvature is negative along the [110] and [111] directions and positive along the [100] direction, leading to an outspread critical field.

These low-field properties are more apparent with Arrott's plots. The behavior is most evident along the [111] direction [Fig. 13(a)], where the linear part leads to a ferromagnetic component ($0.3\mu_B$ at 1.6 K), which disappears between 6 and 7 K [inset of Fig. 13(a)]; the behavior below this linear part and up to 6 K presumably arises from reorientations of the canted magnetic structure under field. In particular, a low critical field seems to exist at 4.2 K around 0.04 T. The behavior is not so clear along the [110] direction, where two different regimes seem to exist, at least between 4 and 8 K [Fig. 13(b)]. Nevertheless, a spontaneous moment of $0.3\mu_B$ can be estimated at 1.6 K. Owing to the low critical field, the situation is more complex for the [100] direction [Fig. 13(c)]. In particular, no spontaneous moment could be detected.

Taking the CEF into account, the Heisenberg and Zeeman couplings as well as the quadrupolar

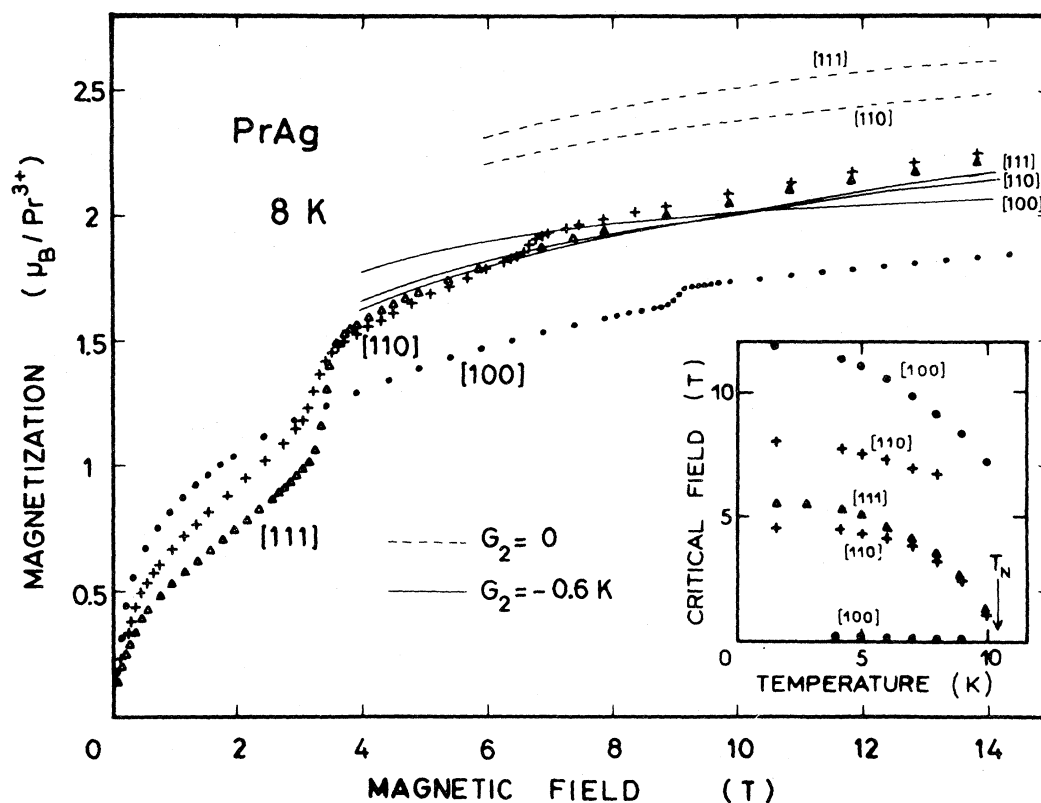


FIG. 11. Magnetization curves along three symmetry directions at 8 K in PrAg; theoretical curves correspond to the same conditions as in Fig. 10. Inset: temperature variation of the critical fields (no value available for the low critical field along [100] below 4 K).

interactions,³⁷ we can try to analyze the high-field magnetization. The calculated curves are drawn in Figs. 10 and 11 with the following hypothesis: All moments are aligned with the applied field; there-

fore the same bilinear exchange parameter as above T_N has been taken ($\Theta^* = 11.5$ K). The CEF and quadrupolar parameters determined above lead to a satisfactory agreement at 1.6 and 8 K for the [110]

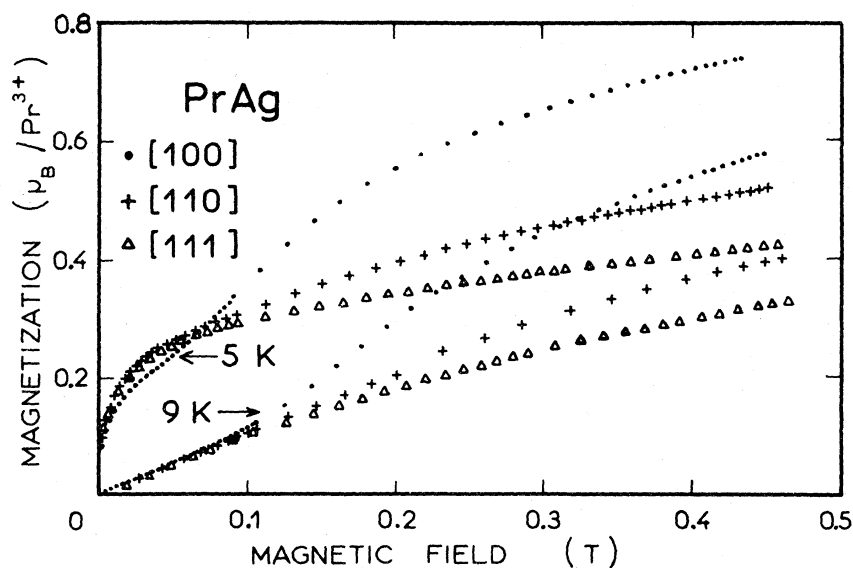


FIG. 12. Low-field magnetization curves along three symmetry directions at 5 and 9 K in PrAg.

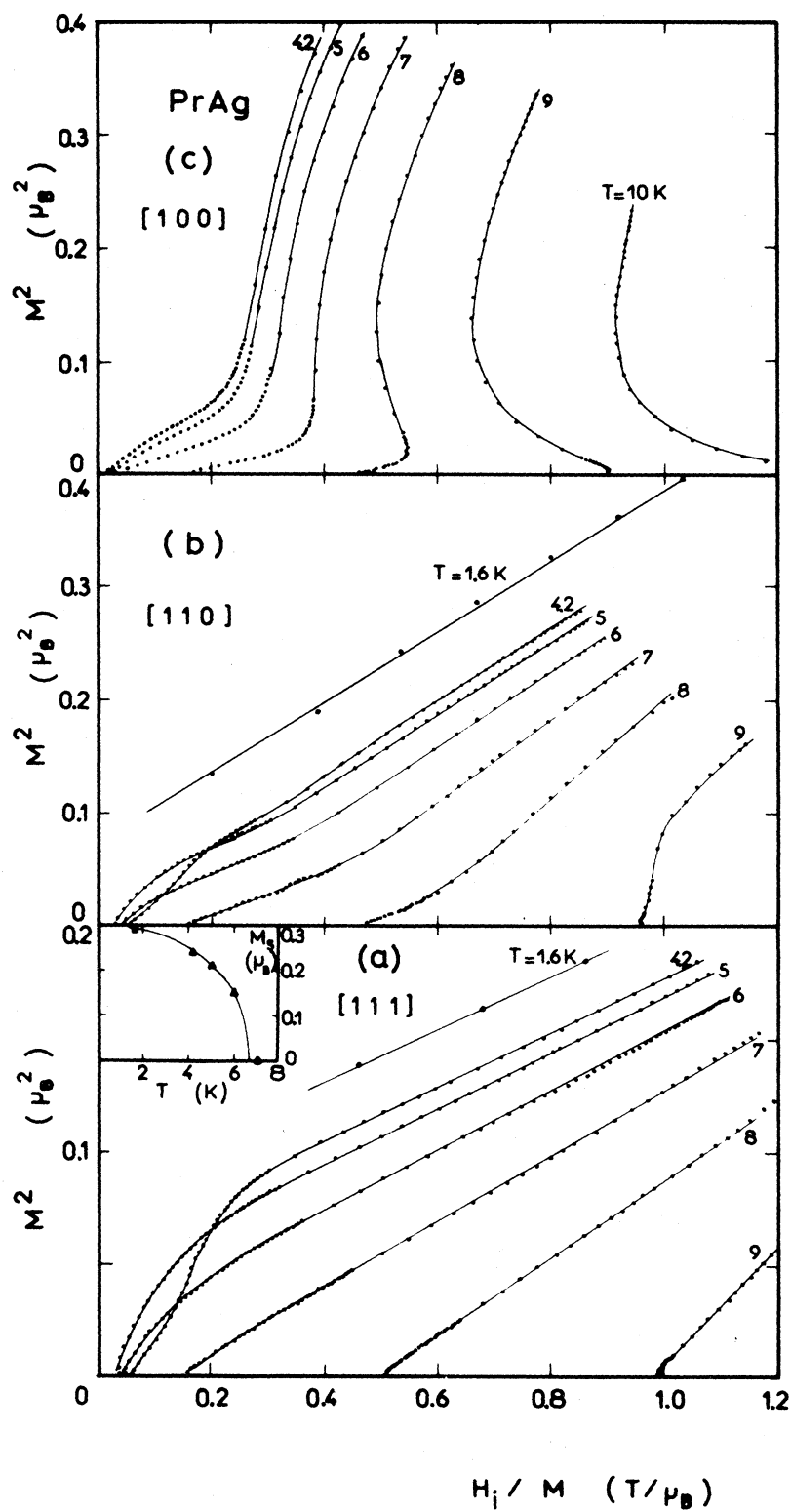


FIG. 13. Arrott's plots along three symmetry directions and at various temperatures in PrAg. Inset of (a): temperature variation of the spontaneous magnetization along [111] (zero-field extrapolation of the linear part); solid lines are only guides for eye.

and [111] directions. This proves the canted structure to be fully closed above the highest critical field. This agreement is also found for the full magnetization curves above T_N .

Along the [100] direction, a large discrepancy occurs with $G_1 = 0$ (only G_1 acts within this symmetry). Taking G_1 values of the order of -0.2 K reduces the magnetization by only $0.1\mu_B$ in 14 T. More negative values seem to be unlikely, because they lead to too large quadrupolar energies, in comparison with the bilinear energy.

IV. DISCUSSION

The main conclusion of this study on poly- and monocrystalline samples of PrAg is the evidence of a slightly canted magnetic structure at low temperature, namely the coexistence of a large antiferromagnetic moment with a small ferromagnetic one. This spontaneous moment vanishes at $T_c = 6.9$ K, the structure remaining purely antiferromagnetic between T_c and T_N .

The actual magnetic structure is not yet fully understood, particularly with regard to the zero-field antiferromagnetic structure (is it collinear or multiaxis?), and solving this problem requires additional studies.

(i) The lack of a sizable spontaneous distortion as it would be expected for a tetragonal magnetic symmetry in CsCl-type rare-earth compounds may indicate the [100] collinear structure to be unlikely. However, a determination of the tetragonal and trigonal magnetoelastic coefficients by parastriction experiments³⁸ would allow to estimate the spontaneous strain for each possible magnetic structure (Fig. 5).

(ii) In order to state the actual structure more precisely, a neutron diffraction study under field would be desirable. Such an experiment has already been performed on a polycrystalline sample,⁶ but with a magnetic field *perpendicular* to the scattering vector. Unfortunately, this configuration is not at all adapted to the case of PrAg, since, in the study of the $(\frac{1}{2}, \frac{1}{2}, 0)$ reflection for example, the field lies in *any direction* within the (110) plane of the crystallites (Ref. 6, Fig. 5). This

field therefore induces spin-flip transitions at different values, according to the crystallite, and the observed variation of intensity results only from an average of all directions of the (110) plane. It would be much better to apply the field *parallel* to the scattering vector, which would allow observation of the behavior of crystallites subject to a field lying along an *unique direction*.

The anisotropy of the magnetocrystalline energy has been calculated to be weak in the same conditions as in Sec. III C. This allows the existence of a canted structure where the resultant magnetic moments do not lie in a principal crystallographic direction. Another consequence is that the high critical fields are mainly due to two-ion couplings. However, from the paramagnetic bilinear exchange parameter $\Theta^* = 11.5$ K and an antiferromagnetic bilinear exchange parameter $\Theta_N^* = 13.5$ K (value which leads to the observed antiferromagnetic ordering at T_N), we deduce a weak antiferromagnetic coupling (~ 2 K). Therefore, we can conclude that the strong negative quadrupolar interactions are probably mainly responsible for the high values of the critical fields as well as the existence of the canted structure.³³ In addition, they favor noncollinear arrangements for the antiferromagnetic moments. A better knowledge of G_1 and G_2 quadrupolar coefficients would be required for selecting the actual structure.

PrAg appears to be the first rare-earth compound where the quadrupolar interactions are strongly negative. Among the two quadrupolar contributions, namely the magnetoelastic and pair couplings, the latter seems to be obviously preponderant, the magnetoelastic contribution being always positive. This predominance of negative quadrupolar pair interactions could be confirmed by performing complementary experiments such as the study of the ultrasonic velocity.

ACKNOWLEDGMENTS

It is a pleasure to thank Dr. R. Aléonard, Dr. Ph. Lethuillier, and Dr. D. Givord for their kind collaboration and many fruitful discussions.

¹C. C. Chao, H. L. Luo, and P. Duwez, *J. Appl. Phys.* **34**, 1971 (1963).

²R. E. Walline and W. E. Wallace, *J. Chem. Phys.* **41**, 3285 (1964).

³J. Pierre and R. Pauthenet, *C. R. Acad. Sci. Paris* **260**, 2739 (1965).

⁴T. O. Brun, G. H. Lander, D. L. Price, G. P. Felcher, and J. F. Reddy, *Phys. Rev. B* **9**, 248 (1974).

- ⁵T. O. Brun, J. S. Kouvel, G. H. Lander, and R. Aitken, *Solid State Commun.* **15**, 1157 (1974).
- ⁶T. O. Brun, J. S. Kouvel, and G. H. Lander, *Phys. Rev. B* **13**, 5007 (1976).
- ⁷K. H. J. Buschow, J. P. de Jong, H. W. Zandbergen, and B. Van Laar, *J. Appl. Phys.* **46**, 1352 (1975).
- ⁸J. W. Cable, W. C. Koehler, and H. R. Child, *J. Appl. Phys.* **36**, 1096 (1965).
- ⁹G. Arnold, N. Nereson, and C. Olsen, *J. Chem. Phys.* **46**, 4041 (1967).
- ¹⁰N. Nereson, in *Magnetism and Magnetic Materials—1972 (Denver)*, Proceedings of the 18th Annual Conference on Magnetism and Magnetic Materials, edited by C. D. Graham and J. J. Rhyne (AIP, New York, 1973), p. 669.
- ¹¹N. Nereson, *J. Appl. Phys.* **44**, 4727 (1973).
- ¹²P. Morin and D. Schmitt, *J. Magn. Magn. Mater.* (in press).
- ¹³D. Schmitt, P. Morin, and J. Pierre, *J. Magn. Magn. Mater.* **8**, 249 (1978).
- ¹⁴R. Takke, N. Dolezal, W. Assmus, and B. Lüthi, *J. Magn. Magn. Mater.* **23**, 247 (1981).
- ¹⁵P. M. Levy, P. Morin, and D. Schmitt, *Phys. Rev. Lett.* **42**, 1417 (1979).
- ¹⁶P. Morin and D. Schmitt, *Phys. Rev. B* **23**, 5936 (1981).
- ¹⁷H. Taub, S. J. Williamson, W. A. Reed, and F. S. L. Hsu, *Solid State Commun.* **15**, 185 (1974).
- ¹⁸C. C. Chao, H. L. Luo, and T. F. Smith, *J. Phys. Chem. Solids* **27**, 1555 (1966); J. S. Schilling, S. Methfessel, and R. N. Shelton, *Solid State Commun.* **24**, 659 (1977).
- ¹⁹R. W. Cohen, G. D. Cody, and J. J. Halloran, *Phys. Rev. Lett.* **19**, 840 (1967).
- ²⁰C. Tannous, D. K. Ray, and M. Belakhovsky, *J. Phys. F* **6**, 2091 (1976).
- ²¹K. R. Lea, M. J. M. Leask, and W. P. Wolf, *J. Phys. Chem. Solids* **23**, 1381 (1962).
- ²²P. Morin, J. Pierre, J. Rossat-Mignod, K. Knorr, and W. Drexel, *Phys. Rev. B* **9**, 4932 (1974).
- ²³D. Schmitt, P. Morin, and J. Pierre, *Phys. Rev. B* **15**, 1698 (1977).
- ²⁴V. U. S. Rao and W. E. Wallace, *Phys. Rev. B* **2**, 4613 (1970).
- ²⁵A. B. Kaiser and S. Doniach, *Int. J. Magn.* **1**, 11 (1970); P. Bossard, J. E. Crow, T. W. Mihalisin, and W. J. L. Buyers, in *Crystalline Electric Field and Structural Effects in f-Electron System*, edited by J. E. Crow, R. P. Guertin, and T. W. Mihalisin (Plenum, New York, 1980), p. 407.
- ²⁶M. Wintenberger and R. Chamard-Bois, *Acta Crystallogr. Sec. A* **28**, 341 (1972).
- ²⁷P. Morin and D. Schmitt, *J. Magn. Magn. Mater.* **21**, 243 (1980).
- ²⁸P. Morin and J. Pierre, *Phys. Status Solidi A* **30**, 549 (1975).
- ²⁹P. Morin, J. Pierre, D. Schmitt, and A. Murani, *Solid State Commun.* **25**, 265 (1978).
- ³⁰P. Morin and J. Pierre, *Phys. Status Solidi A* **21**, 161 (1974).
- ³¹P. Morin, J. Rouchy, and E. du Trémolet de Lacheisserie, *Phys. Rev. B* **16**, 3182 (1977).
- ³²M. Th. Rekveldt, F. J. van Schaik, and W. H. Kraan, *Nukleonika* **24**, 809 (1979); W. H. Kraan and M. Th. Rekveldt, *J. Magn. Magn. Mater.* **8**, 168 (1978).
- ³³J. Sivadrière, *J. Magn. Magn. Mater.* **1**, 23 (1975).
- ³⁴P. A. Fedders and C. W. Myles, *Phys. Rev. B* **19**, 1331 (1979).
- ³⁵J. S. Kouvel, T. O. Brun, and F. W. Korty, *Physica* **86-88B**, 1043 (1977).
- ³⁶J. S. Kouvel and T. O. Brun, *Phys. Rev. B* **22**, 2428 (1980).
- ³⁷C. Jaussaud, P. Morin, and D. Schmitt, *J. Magn. Magn. Mater.* **22**, 98 (1980).
- ³⁸P. Morin, D. Schmitt, and E. du Trémolet de Lacheisserie, *Phys. Rev. B* **21**, 1742 (1980).